Issues in Ultra-Wideband, Widebeam SAR Image Formation

Ron Goodman, Sreenidhi Tummala, Walter Carrara

Environmental Research Institute of Michigan (ERIM)
P.O. Box 134001
Ann Arbor, MI 48113-4001

ABSTRACT

Formation of low-frequency, ultra-wideband/widebeam (UWB/WB) SAR imagery faces inherent challenges not present in conventional SAR systems operating at higher frequencies. Small angle approximations and other shortcuts taken in conventional SAR processors may be inappropriate for the UWB/WB SAR processor. The severe range migration associated with fine resolution UWB/WB SAR poses a significant problem for the image formation algorithm. The combination of a long synthetic aperture and a wide azimuth beamwidth has important implications for motion compensation implementation and performance.

In this paper, we survey the major challenges to UWB/WB SAR image formation. The emphasis here is on formation of fine resolution digital imagery from low frequency UWB/WB data collected in stripmap mode by an airborne SAR system. We examine differences in image formation and data processing between UWB/WB systems and conventional SAR systems. We illustrate aspects of UWB/WB image formation with imagery from the P3 Ultra-Wideband radar system—a 0.3 m resolution SAR which operates in the VHF/UHF frequency bands.

1. INTRODUCTION

Ultra-wideband (UWB) synthetic aperture radar (SAR) is finding important applications in the area of foliage penetration (FOPEN) and as a type of ground penetrating radar (GPR). Most current UWB SAR research activities concentrate on the low frequency (under 2 GHz) region of the electromagnetic spectrum. Low frequency operation, together with fine azimuth resolution (wide azimuth beamwidth), requires the creation of long synthetic apertures or, equivalently, large integration angles. In turn, these large integration angles lead to severe range migration, or motion through resolution cells (MTRC). Scatterers at different locations in an imaged scene experience different levels of MTRC. This variation in MTRC makes selection of the proper image formation algorithm critical. Long synthetic apertures and widebeam (WB) operation have important consequences for implementation and performance of the motion compensation function. Other unique characteristics of UWB/WB imaging also impact image formation processor design.

In this paper, we present issues associated with UWB/WB SAR image formation and propose solutions. Due to space limitations, we do not consider issues related to target scattering, phenomenology, and polarimetric and radiometric calibration. The perspective here is on the formation of fine resolution digital imagery from low frequency UWB/WB data collected in stripmap mode by an airborne SAR sensor.

We illustrate aspects of UWB/WB SAR processing using imagery from the P3 Ultra-Wideband SAR system [1]. The P3 UWB SAR was built by the Environmental Research Institute of Michigan (ERIM) and the Naval Air Warfare Center (NAWC) for the Advanced Research Projects Agency (ARPA). Table 1 summarizes key system parameters. This fully-polarimetric SAR operates in the 215 MHz to 900 MHz region at a 90 degree (broadside) squint angle. It transmits a linear FM (chirp) waveform with 509 MHz bandwidth. Radar echoes are dechirped upon receive, digitized, and recorded on high density digital tape for subsequent ground processing. Image formation is performed on UNIX workstations via the range migration algorithm [2]. Typical image products contain 800 m x 800 m of scene extent with 0.33 m range resolution and 0.66 m azimuth resolution.

Figure 1 shows an example P3 UWB image of the area surrounding a biological experiment station near Pellston, Michigan. Radar illumination and near range are from the left side of the image. This HH polarization image covers a ground area of approximately 800 m in range by 1200 m in azimuth. Figure 2 shows a close-up view of the clearing in the center of the UWB image. The figure identifies two large trihedral reflectors, two trucks, two greenhouses, and an array of plant monitors. The trihedral reflectors, shown in Figure 2(b) and Figure 2(c), help assess image quality. Their large physical size is necessary because of the long wavelength of the P3 UWB system. Figure 1(d) and Figure 1(e) are photographs of two trucks parked in foliage to illustrate FOPEN. Although mostly obscured in the photographs, the trucks are clearly visible through the foliage in the radar image. The point-like scatterers surrounding the clearing result from dihedral reflectors that are formed naturally by tree trunks and the ground.

0-7803-2120-0/95/0000-0479 $4.00 © (1995 IEEE)

Table 1 P3 Ultra-Wideband SAR System Parameters

Parameter	*Value*
Frequency regime	215 - 900 MHz
Transmitted bandwidth	509 MHz
Processed bandwidth	509 MHz
Waveform	Linear FM; dechirp on receive
Range resolution	0.33 m
Azimuth resolution	0.66 m
Recorded swath width	930 m
Center squint angle	90 deg (broadside)
Depression angle	15 - 60 deg
Standoff range	6 - 14 km
Aircraft ground speed	135 m/sec (nominal)
Polarizations	Simultaneous VV, VH, HV, HH
Impulse response	-30 dB Taylor
Antenna	Quad-ridge horn
Image formation	Range migration algorithm
Autofocus	Quadratic mapdrift Phase gradient algorithm

2. CHOICE OF PROCESSING ALGORITHM

The wide coherent angular interval associated with fine resolution WB imaging has a significant impact on the choice of image formation processing (IFP) algorithm. The line-of-sight range to a scatterer varies hyperbolically over a synthetic aperture. For broadside imaging, this variation in range is symmetrical and is known as range curvature. The difficulty with fine resolution imaging, in general, is that this range curvature itself varies with scatterer location in the imaged scene. While it is a straightforward matter to compensate range curvature for a given range bin, it is difficult to compensate range curvature for all range bins simultaneously. For WB imaging, this differential range curvature (DRC) across the imaged swath can be large. When designing a WB SAR system, it is important to select an IFP algorithm that compensates DRC effectively and efficiently.

A number of algorithms are available for fine resolution SAR image formation. The majority of these algorithms use approximations in compensating DRC. These approximations result in residual DRC, and lead to space-variant phase errors which cause defocusing and geometric distortion. As DRC increases in severity, an algorithm's computational complexity increases in order to hold residual errors below some acceptable level.

The range migration algorithm (RMA), also known as the $\Omega - K$ algorithm, is unique in that it provides an exact solution to the problem of DRC [2]. It equalizes the range curvature of all targets via a one-dimensional (range) interpolation. After range curvature equalization, the RMA compresses all targets simultaneously with a single two-dimensional matched filter. The algorithm is computationally efficient, requiring only one-dimensional interpolation and a single matched filter. The RMA is capable of producing large scene, fine resolution UWB/WB imagery in either stripmap or spotlight mode. The output imagery does not suffer geometric distortion or residual phase error from uncompensated range curvature.

3. COHERENT INTEGRATON ANGLE

To achieve azimuth resolution ρ_a, the SAR sensor must observe a target over an angular interval $\Delta\theta$ given by

$$\sin(\Delta\theta/2) = \frac{\lambda k_a}{4\rho_a} \qquad (1)$$

Here λ is the instantaneous transmitted wavelength, k_a is the impulse response (IPR) broadening factor due to aperture weighting (k_a=0.89 for uniform weighting, k_a=1.13 for -30 dB Taylor weighting). The interval $\Delta\theta$ is the coherent integration angle. In stripmap SAR, $\Delta\theta$ is limited to the antenna azimuth beamwidth; in spotlight SAR it is determined by the selected synthetic aperture length.

From (1), the necessary integration angle is proportional to transmitted wavelength. A question arises as to which value of λ to use in (1) when selecting $\Delta\theta$, since the UWB SAR transmits over a wide range of wavelengths. In SAR systems operating at high frequencies, it is natural to select $\Delta\theta$ based on the longest transmitted wavelength (i.e., based on the radar's start frequency). With this definition, we observe adequate target rotation to achieve the desired resolution *at every transmitted wavelength*. For UWB/WB SAR systems which operate at low frequencies, the above definition leads to an impractical wide coherent integration angle. As an example, the P3 UWB SAR would require a 73.3 degree integration angle based on this definition. Instead, we suggest a working definition of azimuth resolution based upon the center wavelength. This definition yields a more practical integration angle of 31.7 degrees for the P3 UWB system at a center frequency of 469.5 MHz.

Selecting $\Delta\theta$ based on the center wavelength rather than the longest wavelength results in an irregularly shaped processing aperture. The origin of this aperture effect is evident in Figure 3, which depicts a signal history aperture in the range/azimuth spatial frequency domain. This "unfilled" aperture causes non-orthogonal sidelobes in the final image. The following section discusses this effect and a method to alleviate it.

4. SIDELOBE CONTROL

Conventional SAR processors typically apply a separable, two-dimensional weighting function (e.g., Taylor) to reduce IPR sidelobe levels at the expense of a slight loss in resolution. The non-rectangular processing aperture shape (unfilled aperture) resulting from the definition of integration angle given above yields unusual sidelobes that are not readily controlled. Figure 4(a) shows an example processing aperture which was simulated based on the parameters in Table 1. Figure 4(b) shows the IPR that results if no weighting (i.e., uniform weighting) is applied. Notice the non-orthogonal sidelobes that appear in addition to the familiar orthogonal sidelobes. The non-orthogonal sidelobes result from the missing corners of the processing aperture. Figure 4(c) shows a result in which the unfilled aperture has been Taylor weighted (-30 dB) in the usual, separable manner. Although the orthogonal sidelobes have been suppressed to the -30 dB level, the non-orthogonal sidelobes remain present.

A simple method we refer to as *variable weighting* is capable of suppressing the non-orthogonal sidelobes in Figure 4(b). In this approach, which is also separable, a variable length weighting vector is generated for each range or azimuth record based on the amount of data available in that particular record. The weighting vector is centered on the available (nonzero) data to which it is applied. Figure 4(d) displays the IPR which results when this variable weighting scheme is applied to the aperture of Figure 4(a). The orthogonal sidelobes have again been controlled, and the non-orthogonal sidelobes are now suppressed as well.

5. MOTION COMPENSATION

Consider the simple case of a two-dimensional (slant plane) geometry with perfect motion measurement capability. This data collection geometry is shown in Figure 5. We wish to process imagery from a strip of range width W_S in azimuth batches of length W_A. This batch processing procedure is consistent with many stripmap image formation algorithms, including the range migration algorithm discussed above. We assume the data is demodulated in range using a constant reference time delay ($2R_o/c$) for all pulses over the entire data collection time. The quantity R_o is the broadside range to the center of the imaged swath.

A motion compensation difficulty arises in WB SAR systems. The angular interval through which targets must be observed is defined by (1) above. Referring to Figure 6, a cross track motion of ΔY causes a phase effect of $4\pi\Delta Y/\lambda$ radians for targets at beam center and $4\pi\Delta Y\cos(\Delta\theta/2)/\lambda$ radians for targets at the edges of the required beamwidth. In conventional stripmap motion compensation procedures, all targets in a returned pulse are adjusted identically (for the broadside or beam center target). This procedure results in a phase effect given by

$$\Phi_e = \frac{4\pi\Delta Y}{\lambda}(1-\cos(\Delta\theta/2)) \qquad (2)$$

for target returns from the edges of the beam. Following this usual motion compensation procedure, the average phase effect is approximately the same for all targets in the scene. How Φ varies over the azimuth processing time (that is, linear, quadratic, or higher order) depends on how ΔY varies with time. As a quantitative example, for ΔY=2 m, λ=0.64 m, and $\Delta\theta$=31.7 degrees, we have Φ=85.7 degrees, a noticeable azimuth phase error. More extreme cross-track variations result in many wavelengths of azimuth phase error. Again, this error exists even with perfect measurement of sensor deviations from a straight line.

We offer a second approach to implement phase adjustments for measured motions in a way to significantly reduce residual motion-induced phase effects. This approach is consistent with dividing the strip into azimuth subpatches of length W_A as before. In this case, however, we first motion compensate the signal data to scene center rather than to the instantaneous broadside target (the conventional stripmap technique). We then reinstate the azimuth chirp corresponding to an ideal, straight-line flight path. The signal is now ready for the standard range migration processing procedures with small residual motion effects.

While there is large overlap in the data processed for each azimuth subpatch, we must motion compensate the data differently (and separately) for each processed subpatch in this second approach. The choice of subpatch size greatly impacts processor efficiency.

With this second approach, it can be shown that the maximum residual phase effect (Φ_e) varies over the scene, from zero at subpatch center to

$$\Phi_e = \pi\Delta Y\frac{k_a W_A^2}{8R_o^2\rho_a}\frac{(\cos(\Delta\theta/2))^3}{\sin(\Delta\theta/2)} \qquad (3)$$

for a target at an azimuth edge of the subpatch. This quantity is relatively small for a reasonable size of W_A and other parameter values considered here.

6. AUTOFOCUS

Conventional SAR systems often treat motion-induced phase errors as a one-dimensional problem. A number of robust autofocus techniques exist which are able to estimate quadratic and higher order azimuthal phase errors in SAR data. The usual compensation approach is to

apply the same error correction at all wavelengths, even though the magnitude of the phase error varies with wavelength according to

$$\Phi(\lambda, x) = \frac{4\pi\Delta R(x)}{\lambda} \quad (4)$$

where x is along track sensor position, and $\Delta R(x)$ represents an uncompensated motion over the processing aperture. Due to the high fractional bandwidth of UWB SAR, the two-dimensional nature of phase errors may not be negligible.

Correcting the phase error described by (3) is not difficult if the error is known at a specific wavelength. By performing autofocus in the range compressed signal history domain, we naturally estimate the azimuthal phase error at the center wavelength. The phase error estimate is then scaled with wavelength to form a two-dimensional error estimate described by

$$\Phi_{2D}(\lambda, x) = \left(\frac{\lambda_c}{\lambda}\right)\hat{\Phi}(\lambda, x) \quad (5)$$

where λ_c is the center wavelength, and $\hat{\Phi}(\lambda, x)$ is the error estimate obtained from a conventional autofocus algorithm, such as mapdrift or the phase gradient algorithm. A multiplicative correction function is obtained as $\exp\{-j\Phi_{2D}(\lambda, x)\}$, which is then applied to the fully uncompressed signal history.

7. RF INTERFERENCE

A final problem in low frequency UWB SAR is the presence of dominant interfering RF signals. These signals originate from a number of sources, the most serious being VHF and UHF television transmitters and cellular telephones. Figure 7 shows an example spectrum plot taken from the same geographic area as the image of Figure 1. The power spectrum was measured by recording data through the P3 UWB receiver with the transmitter turned off.

Figure 8(a) shows a SAR image from the 450-600 MHz region which exhibits severe degradation due to RFI. To improve this image, a simple filtering scheme was employed to remove most of the interference energy prior to image formation. Figure 8(b) shows the result of this simple RF suppression algorithm. Investigation into efficient and robust techniques for suppressing RFI remains an active area of research.

CONCLUSIONS

The high range bandwidth and large azimuth beamwidth associated with fine resolution, low frequency SAR systems present a number of practical issues for the digital image formation processor. An additional concern is the presence of inband RF interference and its resultant image quality degradation. New processing algorithms and modifications of conventional techniques are required to address these issues.

ACKNOWLEDGMENTS

We wish to express our appreciation to Dr. Dom Giglio of ARPA and Mr. James Verdi of NAWC for their support and participation in the P3 UWB upgrade effort.

REFERENCES

1. Sheen, D.R., C.M. Strawitch, and T.B. Lewis, "UHF Wideband SAR Design and Preliminary Results," *Proceedings of the 1994 IEEE International Geoscience and Remote Sensing Symposium (IGARSS)*, Pasadena, CA, August 1994.

2. Cafforio, C., C. Prati, and F. Rocca, "SAR Data Focusing using Seismic Migration Techniques," *IEEE Transactions on Aerospace and Electronic Systems*, Vol. 27, No. 2, March 1991.

Figure 1 Example SAR image from P3 UWB system.

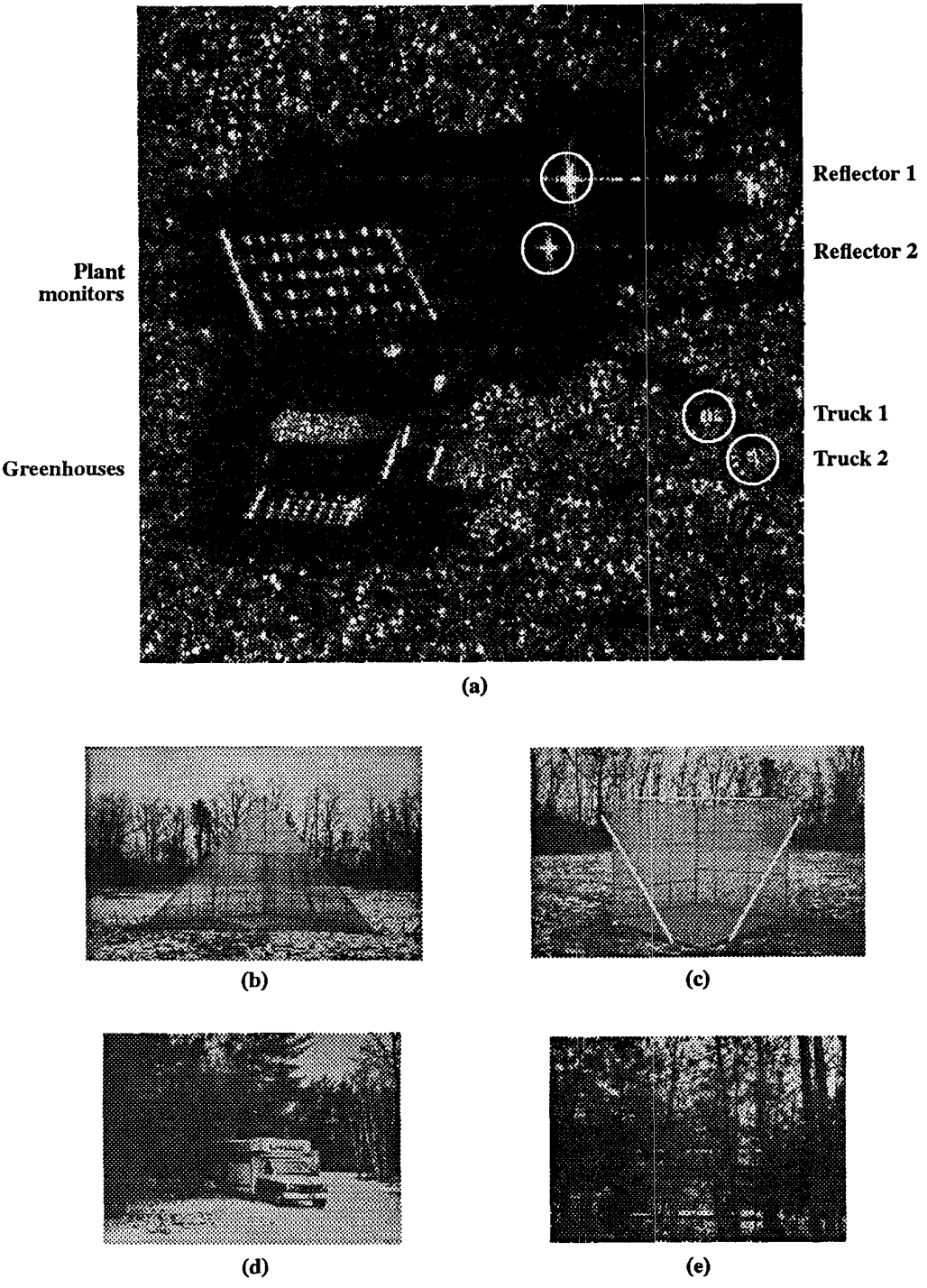

Figure 2 Expanded view of clearing in P3 UWB image **(a)** SAR image; **(b)** Reflector 1 (trihedral with 4.9 m sides); **(c)** Reflector 2 (trihedral with 2.5 m sides); **(d)** Truck 1; **(e)** Truck 2.

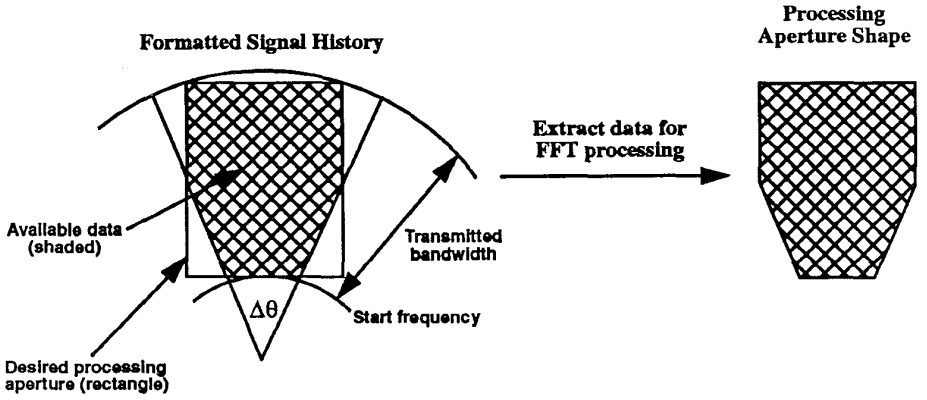

Figure 3 UWB/WB SAR processing aperture shape.

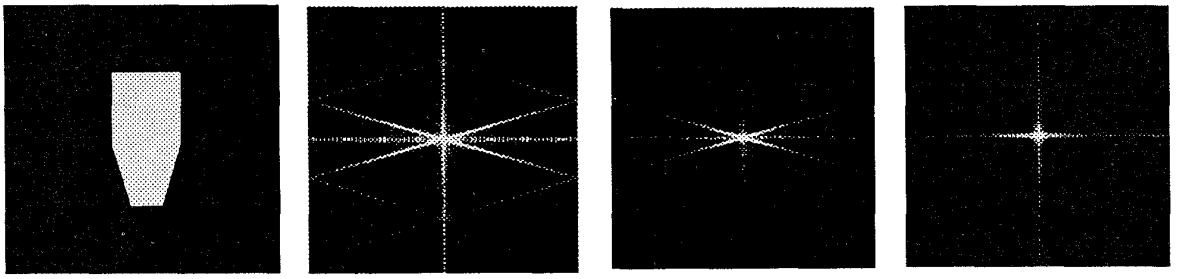

Figure 4 Simulated UWB/WB SAR impulse response **(a)** Signal aperture support; **(b)** Uniform weighting; **(c)** Conventional -30 dB Taylor weighting; **(d)** Variable -30 dB Taylor weighting.

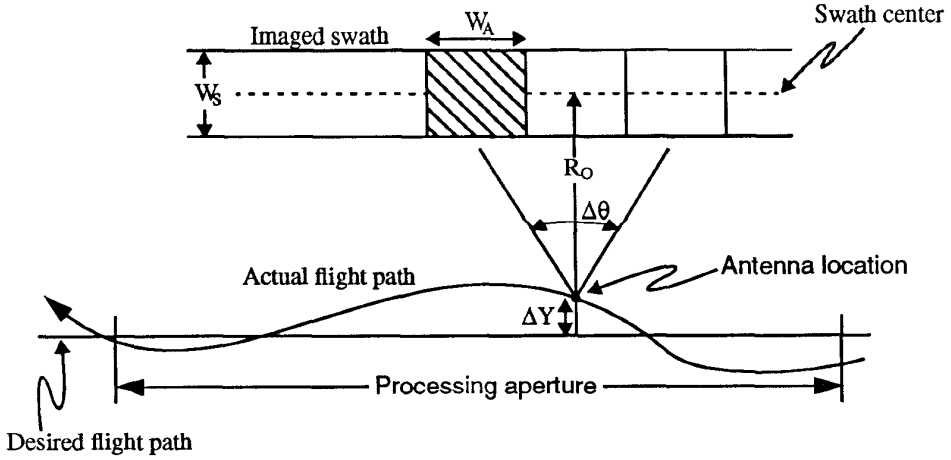

Figure 5 Stripmap SAR imaging geometry.

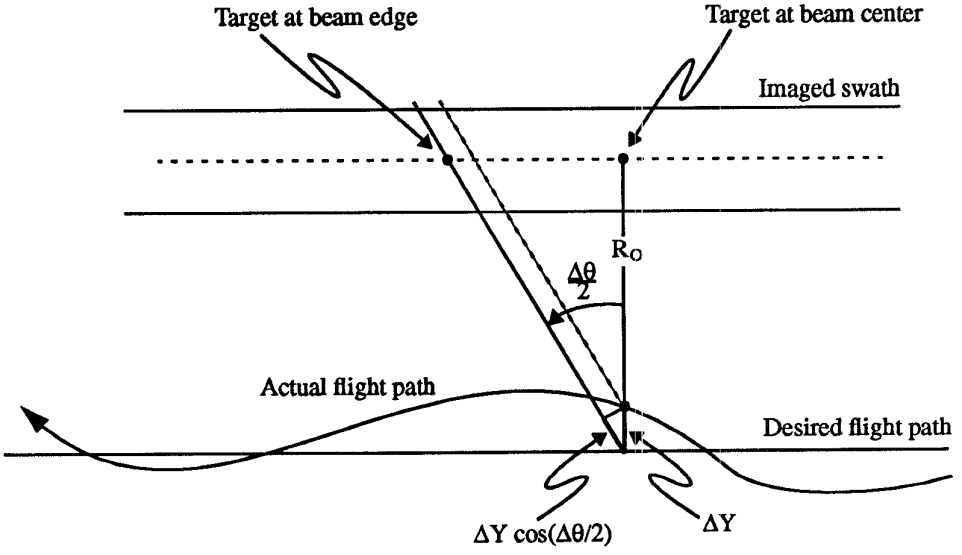

Figure 6 Motion compensation requirement for widebeam SAR.

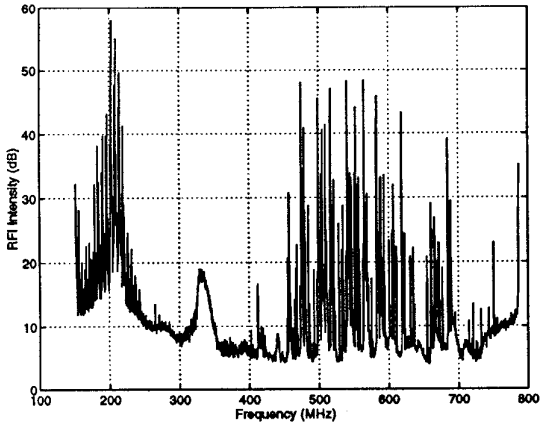

Figure 7 RF interference power spectrum.

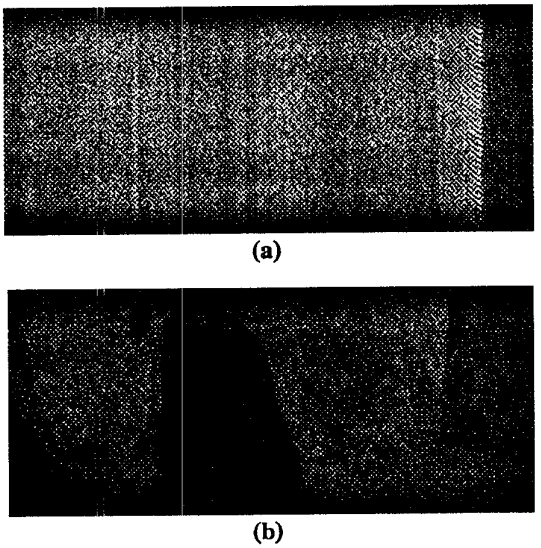

(a)

(b)

Figure 8 Example of RFI suppression **(a)** Image degraded by severe RFI; **(b)** Image after RFI suppression.